

# Majorana representation, qutrit Hilbert space and NMR implementation of qutrit gates

Shruti Dogra,<sup>\*</sup> Kavita Dorai,<sup>†</sup> and Arvind<sup>‡</sup>

*Department of Physical Sciences, Indian Institute of Science Education & Research Mohali,  
Sector 81 SAS Nagar, Manauli PO 140306 Punjab India.*

We use the Majorana geometrical representation for a qutrit, where a pair of points on a unit sphere represents its quantum states. A canonical form for qutrit states is presented, where every qutrit state can be obtained from a one-parameter family of states via  $SO(3)$  action. The notion of spin-1 magnetization which is invariant under  $SO(3)$ , is discussed and geometrically interpreted on the Majorana sphere. We study the dynamics of the pair of points representing a qutrit state under various useful quantum operations and connect them to different NMR operations. In our scheme, the rigid rotation of this pair of points under  $SO(3)$  corresponds to non-selective pulses in NMR, while transition-selective NMR pulses are generated by the eight generators of  $SU(3)$  and typically lead to the movement of only one point at a time on the Majorana sphere. Using the Majorana picture, we also describe the action of several quantum gates and the insights gained, are used to perform experiments on a spin-1 system (the NMR qutrit) oriented in a liquid crystalline environment. Finally, using the Gell Mann matrix picture we describe and experimentally implement a scheme for complete qutrit state tomography.

PACS numbers: 03.67.Lx, 03.67.Bg

## I. INTRODUCTION

The Bloch sphere provides a representation of the quantum states of a single qubit onto  $S^2$  (a unit sphere in three real dimensions), with pure states mapped onto the surface and the mixed states lying in the interior [1, 2]. This geometrical representation is useful in providing a visualization of quantum states and their transformations, particularly in the case of NMR-based quantum computation, where the spin- $\frac{1}{2}$  magnetization and its transformation through NMR rf pulses is visualized on the Bloch sphere [3]. There have been several proposals for the geometrical representation for higher-level quantum systems [4–11] however, extensions of a Bloch sphere-like picture to higher spins is not straightforward. A geometrical representation was proposed by Majorana in which, a pure state of a spin ‘ $s$ ’ is represented by ‘ $2s$ ’ points on the surface of a unit sphere, called the Majorana sphere [12]. The Majorana representation for spin- $s$  systems has found widespread applications such as determining geometric phase of spins [13, 14], representing  $N$  spinors by  $N$  points [15], geometrical representation of multi-qubit entangled states [16–18], statistics of chaotic quantum dynamical systems [19] and characterizing polarized light [20].

A single qutrit (three-level quantum system) is of particular importance in qudit-based ( $d$ -level quantum system) quantum computing schemes [21–27]. A qutrit is the smallest system that exhibits inherent quantum features such as contextuality [28–30], which has been con-

jectured to be a resource for quantum computing [31–33]. NMR qudit quantum computing can be performed by using nuclei with spin  $> \frac{1}{2}$  or can be modeled by two or more coupled spin- $\frac{1}{2}$  nuclei [34, 35].

In this work we use the Majorana sphere description of a single qutrit, where states of a qutrit are represented by a pair of points on a unit sphere, to provide insights into the qutrit state space. The group of unitary transformations  $SU(3)$  and the group of rotations in three dimensions  $SO(3)$  play an important role in the study of a qutrit. We propose a way to parameterize single-qutrit states, where arbitrary qutrit states are generated from a one-parameter family of a canonical subset of states via the action of  $SO(3)$  transformations. The unitary transformation corresponding to the physical rotations represented by  $SO(3)$  act rigidly on the Majorana sphere. The  $SO(3)$  invariant notion of spin magnetization finds a natural representation on the Majorana sphere. States are identified as “pointing” or “non-pointing”, depending upon the zero or non-zero value of the spin magnetization. As the state of a qutrit evolves, the pair of points representing the state moves on the surface of the Majorana sphere. The physical rotations represented by  $SO(3)$  when implemented unitarily, and which correspond to rigid rotations of the pair of points on the Majorana sphere are experimentally realized in NMR via spin-selective pulses. The transformation generated by the standard  $SU(3)$  generators given by  $\Lambda$ -matrices [4] correspond in most cases to the movement of only one point on the Majorana sphere, and are experimentally realized in NMR via transition-selective pulses.

The above correspondences are used to visualize and experimentally implement different gates on a qutrit that are used in NMR quantum computing, namely SWAP gates, controlled-phase shift gates and a three-dimensional analogue of the Hadamard gate. We used a

<sup>\*</sup> shrutidogra@iisermohali.ac.in

<sup>†</sup> kavita@iisermohali.ac.in

<sup>‡</sup> arvind@iisermohali.ac.in

spin-1 deuterium nucleus of a chloroform-D molecule to realize an NMR qutrit. In order to obtain a well resolved pair of single-quantum transitions in the deuterium NMR spectrum, the chloroform-D molecule is embedded in an anisotropic liquid crystalline environment. The experimental implementation of these ternary quantum gates is validated by complete quantum state tomography which we carry out using the Gell Mann matrices.

The material in this paper is arranged as follows: Section II contains a discussion of the Majorana representation of a spin-1 particle, while section III focuses on the dynamics of a spin-1 particle under  $SU(3)$  and  $SO(3)$  operations. The canonical state transformations and the Majorana representation of the spin-1 magnetization vector are described in sections III A and III B, respectively. Section IV describes the basic requirements to perform NMR quantum computing using a single qutrit. The qutrit system, initialization scheme, quantum gate realizations and experimental NMR implementations of qutrit gates are described in sections IV A - IV D, respectively. Section V contains a few concluding remarks.

## II. MAJORANA REPRESENTATION

In the Majorana representation each state of a spin- $s$  quantum system is represented by  $2s$  points on the surface of a unit sphere [12]. Consider the  $2s + 1$  orthonormal eigen vectors of the angular momentum operator  $L_z$ ,  $\{|j\rangle\}$  with  $j$  ranging from  $-s$  to  $+s$ , providing a basis for the Hilbert space of spin  $s$ . The most general quantum pure state for the system is given in terms of  $2s + 1$  complex coefficients  $C_j$  as

$$|\Psi\rangle = \sum_{j=-s}^{+s} C_j |j\rangle = C_{-s} | -s\rangle \cdots + C_0 |0\rangle \cdots + C_{+s} | +s\rangle \quad (1)$$

with  $\sum_{j=-s}^s |C_j|^2 = 1$ . Majorana introduced a polynomial of degree  $2s$  whose coefficients are derived from the expansion coefficients given in Eqn.(1),

$$a_0 \zeta^{2s} + a_1 \zeta^{2s-1} + \dots + a_{2s} = 0, \quad (2)$$

$$a_r = (-1)^r \frac{C_{s-r}}{\sqrt{(2s-r)!r!}}.$$

This polynomial has  $2s$  complex roots which are determined by the coefficients  $C_j$  and completely determine the quantum state of the spin  $s$  system, upto an overall phase. These points are plotted in the complex  $xy$ -plane and the inverse stereographic projection of these roots with respect to the south pole gives us  $2s$  points on the surface of a unit sphere. These  $2s$  points provide the Majorana representation of the state  $|\psi\rangle$ .

For the specific case of a qutrit that interests us, the three-dimensional Hilbert space is spanned by the three eigen vectors  $\{|-1\rangle, |0\rangle, |+1\rangle\}$  of the angular momentum operator  $\Sigma_3$  ( $L_z$ ). The general state is given by

$$|\Psi\rangle = C_{-1} |-1\rangle + C_0 |0\rangle + C_{+1} |+1\rangle \quad (3)$$

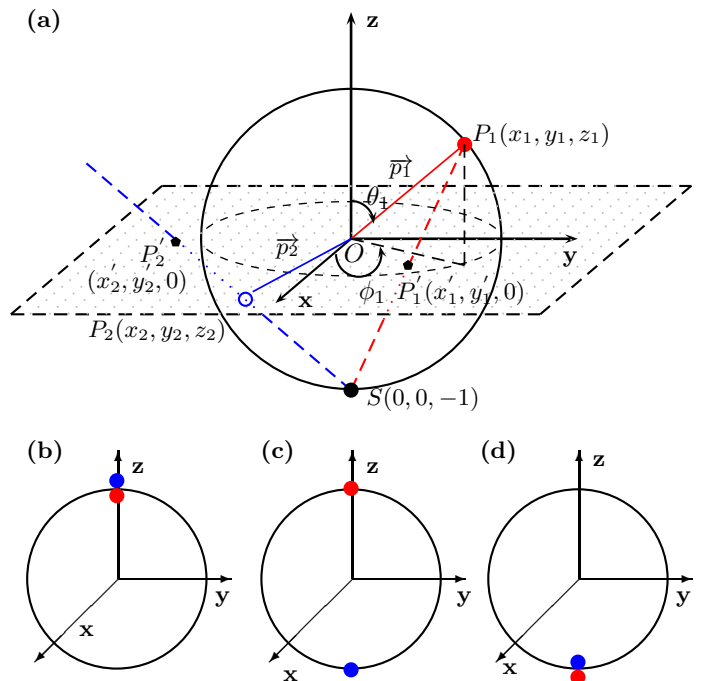


FIG. 1. A qutrit on the Majorana sphere is represented by two points  $P_1$  and  $P_2$ , connected with the center of the sphere by lines shown in red and blue respectively.  $\theta_1, \phi_1$  are the polar and azimuthal angles corresponding to point  $P_1$  ( $\theta_2, \phi_2$  are the angles for point  $P_2$ ). (a) Roots of the Majorana polynomial are shown in the plane  $z = 0$  by points  $P'_1$  and  $P'_2$ , whose stereographic projection give rise to the Majorana representation. Three examples are shown corresponding to the Majorana representation of single-qutrit basis vectors (b)  $|+1\rangle$ , (c)  $|0\rangle$  and (d)  $|-1\rangle$ .

and the corresponding Majorana polynomial is a quadratic equation. Fig. 1(a) shows the Majorana sphere representation of a qutrit, with the roots of the Majorana polynomial shown as points  $P'_1(x'_1, y'_1, 0)$  and  $P'_2(x'_2, y'_2, 0)$ . The corresponding points obtained via inverse stereographic projections with respect to the south pole are shown as points  $P_1$  and  $P_2$ , and they determine the quantum state of a qutrit system in the Majorana representation. The three basis states are shown on the Majorana sphere in Figs. 1(b)-(d) respectively. The Majorana representation of  $|+1\rangle$  consists of the points  $(0, 0, 1)$  and  $(0, 0, 1)$  which are overlapping points on the north pole. Similarly, for the state  $|-1\rangle$ , both the points lie on the south pole. For the state  $|0\rangle$ , one point lies on the north pole while the other point lies on the south pole. In general, the points  $P_1$  and  $P_2$  can lie anywhere on the sphere and we can find such a representation for every pure quantum state of a qutrit.

Let us consider two arbitrary points  $P_1(\theta_1, \phi_1)$  and  $P_2(\theta_2, \phi_2)$  on the Majorana sphere with  $\theta_i \in [0, \pi]$  and  $\phi_i \in [0, 2\pi]$ . Fig. 1(a) shows these points as well as their stereographic projections from the south pole. The corresponding points  $P'_1$  and  $P'_2$  in the complex plane are also shown. The coordinates of these points  $P'_i$ ,  $i = 1, 2$

in the complex plane in terms of the polar coordinates of  $P_1$  and  $P_2$  are given by

$$\begin{aligned} x'_i &= (\sin \theta_i \cos \phi_i)/(1 + \cos \theta_i) \\ y'_i &= (\sin \theta_i \sin \phi_i)/(1 + \cos \theta_i) \end{aligned} \quad (4)$$

Thus the two roots of the second degree Majorana polynomial for a qutrit are  $e^{\iota \phi_i} \tan \frac{\theta_i}{2}$ ,  $i = 1, 2$ . From the roots we find the coefficients of the quadratic Majorana polynomial and the most general qutrit state:

$$|\psi_g\rangle = \Gamma \begin{pmatrix} \sqrt{2} \cos \frac{\theta_1}{2} \cos \frac{\theta_2}{2} \\ e^{\iota \phi_1} \sin \frac{\theta_1}{2} \cos \frac{\theta_2}{2} + e^{\iota \phi_2} \cos \frac{\theta_1}{2} \sin \frac{\theta_2}{2} \\ \sqrt{2} e^{\iota(\phi_1 + \phi_2)} \sin \frac{\theta_1}{2} \sin \frac{\theta_2}{2} \end{pmatrix}$$

$$\Gamma = \sqrt{2} [3 + \cos \theta_1 \cos \theta_2 + \sin \theta_1 \sin \theta_2 \cos(\phi_1 - \phi_2)]^{-\frac{1}{2}}$$

$$\theta_i \in [0, \pi], \quad \phi_i \in [0, 2\pi], \quad i = 1, 2. \quad (5)$$

As evident from Eqn. (5), a pure state of a single qutrit is represented by six real (three complex) parameters; using one normalization condition reduces this number to five and with the states being defined upto an overall phase, the number of parameters determining a general pure qutrit state reduces to four.

### III. $SU(3)$ AND $SO(3)$ CANONICAL STATES AND INVARIANT MAGNETIZATION

The group of unitary transformation in three dimensions  $SU(3)$  and the group of rotations in three dimensions  $SO(3)$  (embedded in  $SU(3)$  as a subgroup) play an important role in the study of a qutrit. A convenient set of generators for the group  $SU(3)$  is provided by the Lambda matrices due to Gell Mann.

$$\begin{aligned} \Lambda_1 &= \begin{pmatrix} 0 & 1 & 0 \\ 1 & 0 & 0 \\ 0 & 0 & 0 \end{pmatrix}, \Lambda_2 = \begin{pmatrix} 0 & -\iota & 0 \\ \iota & 0 & 0 \\ 0 & 0 & 0 \end{pmatrix}, \Lambda_3 = \begin{pmatrix} 1 & 0 & 0 \\ 0 & -1 & 0 \\ 0 & 0 & 0 \end{pmatrix}, \\ \Lambda_4 &= \begin{pmatrix} 0 & 0 & 1 \\ 0 & 0 & 0 \\ 1 & 0 & 0 \end{pmatrix}, \Lambda_5 = \begin{pmatrix} 0 & 0 & -\iota \\ 0 & 0 & 0 \\ \iota & 0 & 0 \end{pmatrix}, \Lambda_6 = \begin{pmatrix} 0 & 0 & 0 \\ 0 & 0 & 1 \\ 0 & 1 & 0 \end{pmatrix}, \\ \Lambda_7 &= \begin{pmatrix} 0 & 0 & 0 \\ 0 & 0 & -\iota \\ 0 & \iota & 0 \end{pmatrix}, \quad \Lambda_8 = \frac{1}{\sqrt{3}} \begin{pmatrix} 1 & 0 & 0 \\ 0 & 1 & 0 \\ 0 & 0 & -2 \end{pmatrix}. \end{aligned} \quad (6)$$

The transformations that these matrices generate upon exponentiation are given by

$$U_{\Lambda_i} = e^{\iota \theta \Lambda_i} \quad (7)$$

and they target a two-level subspace of the three-level quantum system. These operations can be experimentally implemented via transition-selective pulses in NMR, which are governed by the single transition operators [36], generating transformations:

$$e^{\iota \xi I_k^{rs}} = I - I^{rs} + \cos \frac{\xi}{2} I_k^{rs} + 2\iota \sin \frac{\xi}{2} I_k^{rs} \quad (8)$$

which are unitary operators exciting transitions between levels  $r, s$  about the  $k^{th}$  axis by an angle  $\xi$ .  $I_k^{rs}$  is the product operator element corresponding to the  $(r, s)$  subspace and  $k \in \{x, y, z\}$ . A direct connection between single-transition operators in NMR and the Gell Mann matrices can be established:

$$\begin{aligned} I_x^{12} &= \frac{1}{2} \Lambda_1, & I_y^{12} &= \frac{1}{2} \Lambda_2, & I_z^{12} &= \frac{1}{2} \Lambda_3 \\ I_x^{23} &= \frac{1}{2} \Lambda_6, & I_y^{23} &= \frac{1}{2} \Lambda_7, & I_z^{23} &= \frac{1}{2} (\sqrt{3} \Lambda_8 - \Lambda_3) \\ I_x^{13} &= \frac{1}{2} \Lambda_4, & I_y^{13} &= \frac{1}{2} \Lambda_5, & I_z^{13} &= \frac{1}{2} (\sqrt{3} \Lambda_8 + \Lambda_3) \end{aligned} \quad (9)$$

The above connection leads to the possibility of implementing transformations generated by Gell Mann matrices via rf pulses on single transitions. The transformations corresponding to the indices (13) in Equation (9) are associated with a double-quantum transition and cannot be implemented by one rf pulse on a single transition and instead involve cascades of pulses [39].

The group  $SO(3)$  plays a very important role in qutrit physics: on the one hand it acts as the group of rotations in three dimensions and on the other it is a subgroup of  $SU(3)$  through its spin 1 unitary representation. The generators of this group in its defining representation denoted by  $J_j$  and in its three dimensional unitary representation denoted by  $\Sigma_j$  are given by

$$\begin{aligned} J_1 &= i \begin{pmatrix} 0 & 0 & 0 \\ 0 & 0 & 1 \\ 0 & -1 & 0 \end{pmatrix}, & \Sigma_1 &= \frac{1}{\sqrt{2}} \begin{pmatrix} 0 & 1 & 0 \\ 1 & 0 & 1 \\ 0 & 1 & 0 \end{pmatrix}, \\ J_2 &= i \begin{pmatrix} 0 & 0 & 1 \\ 0 & 0 & 0 \\ -1 & 0 & 0 \end{pmatrix}, & \Sigma_2 &= \frac{1}{\sqrt{2}} \begin{pmatrix} 0 & -\iota & 0 \\ \iota & 0 & -\iota \\ 0 & \iota & 0 \end{pmatrix}, \\ J_3 &= i \begin{pmatrix} 0 & -1 & 0 \\ 1 & 0 & 0 \\ 0 & 0 & 0 \end{pmatrix}, & \Sigma_3 &= \begin{pmatrix} 1 & 0 & 0 \\ 0 & 0 & 0 \\ 0 & 0 & -1 \end{pmatrix} \end{aligned} \quad (10)$$

The generators  $J_j$  generate finite rotations about the  $x, y$  and  $z$  axes respectively while the generators  $\Sigma_j$  generate the corresponding three dimensional unitary transformations:

$$R_j(\xi) = e^{i\xi J_j} \in SO(3); \quad U_j(\xi) = e^{i\xi \Sigma_j} \in SO(3) \subset SU(3) \quad (11)$$

When the group  $SO(3)$  acts on the real physical space via its defining representation and the corresponding action on quantum states is via its unitary representation, the points on the Majorana sphere transform rigidly and as per the defining representation of  $SO(3)$ . This is a very useful feature and can be exploited in describing and transforming quantum states of the qutrit.

Consider a single-qutrit state,  $|\psi_{initial}\rangle$  whose Majorana representation is given as points  $P_1(x_1, y_1, z_1)$  and  $P_2(x_2, y_2, z_2)$  (Fig. 1(a)). Joining each of these points with the center of the sphere  $O(0, 0, 0)$ , one obtains unit vectors  $\overrightarrow{OP_1}$  and  $\overrightarrow{OP_2}$ , which are represented as  $\vec{p}_1$

and  $\vec{p}_2$  respectively in Fig. 1(a). Under the  $SO(3)$  action these vectors rotate together and rigidly while the quantum state in the Hilbert space undergoes the corresponding unitary transformation

$$U_i(\xi) = e^{i\xi\Sigma_i} = I + (\cos \xi - 1) \Sigma_i^2 + i \sin \xi \Sigma_i \quad (12)$$

where  $I$  is the  $3 \times 3$  identity matrix. When  $U_i(\xi)$  acts on a single-qutrit state  $|\psi\rangle$  in the 3-dimensional Hilbert space, it leads to the rotation of the two points representing a qutrit on the Majorana sphere by angle  $\xi$  about  $i$ -axis.

To illustrate this let us consider a general single-qutrit state ( $|\psi_g\rangle$ ) given in Eqn. (5) as the initial state ( $|\psi_{initial}\rangle$ ). The Majorana representation of this state is given by two points:  $P_1(\sin \theta_1 \cos \phi_1, \sin \theta_1 \sin \phi_1, \cos \theta_1)$  and  $P_2(\sin \theta_2 \cos \phi_2, \sin \theta_2 \sin \phi_2, \cos \theta_2)$ . Considering an operator  $U_z(\xi_z = \phi_1)$ , under whose action the general single-qutrit state gives rise to the final state:

$$|\psi_{final}\rangle = \Gamma \begin{pmatrix} \sqrt{2} \cos \frac{\theta_1}{2} \cos \frac{\theta_2}{2} \\ \sin \frac{\theta_1}{2} \cos \frac{\theta_2}{2} + e^{i(\phi_2 - \phi_1)} \cos \frac{\theta_1}{2} \sin \frac{\theta_2}{2} \\ \sqrt{2} e^{i(\phi_2 - \phi_1)} \sin \frac{\theta_1}{2} \sin \frac{\theta_2}{2} \end{pmatrix}$$

$$\Gamma = \frac{\sqrt{2}}{\sqrt{3 + \cos \theta_1 \cos \theta_2 + \sin \theta_1 \sin \theta_2 \cos(\phi_1 - \phi_2)}}. \quad (13)$$

Majorana representation of state  $|\psi_{final}\rangle$  is given by the points:  $Q_1(\sin \theta_1, 0, \cos \theta_1)$  and  $Q_2(\sin \theta_2 \cos(\phi_2 - \phi_1), \sin \theta_2 \sin(\phi_2 - \phi_1), \cos \theta_2)$ . These points are the same as those obtained from  $(P_1, P_2)$  by the direct action of the group  $SO(3)$  via its defining representation. Interestingly, the  $SO(3)$  transformations on a single qutrit are experimentally implemented by a non-selective rf pulse in NMR which is in contrast to the transformations generated by the Gell Mann matrices where single transition pulses are involved.

### A. Canonical states

Can the  $SO(3)$  transformations described above be used to develop a convenient parameterization of the qutrit states? It turns out that we can obtain all the states of a qutrit from a one-parameter family of states via the  $SO(3)$  action. Consider a one-parameter family of states described by a real parameter  $\alpha$ :

$$|\psi_c\rangle = \begin{pmatrix} \sin \alpha \\ 0 \\ \cos \alpha \end{pmatrix} \quad \text{where } \alpha \in [0, \pi/2] \quad (14)$$

Majorana representation of  $|\psi_c\rangle$  consists of two points,  $P_1(0, y_c, z_c)$  and  $P_2(0, -y_c, z_c)$  where  $y_c = \frac{\sqrt{2} \sin 2\alpha}{\sin \alpha + \cos \alpha}$  and  $z_c = \frac{\sin \alpha - \cos \alpha}{\sin \alpha + \cos \alpha}$ . These points lie on the great circle in the plane  $x = 0$ , such that they have same value of  $z$ -coordinates and equal and opposite values of the

projection on  $y$ -axis as shown in Fig. 2 and the angle enclosed between the points  $P_1$  and  $P_2$  at the center of sphere is  $\eta = 2 \sin^{-1} y_c$ . As  $\alpha$  varies from  $0 \leq \alpha \leq \frac{\pi}{2}$ ,

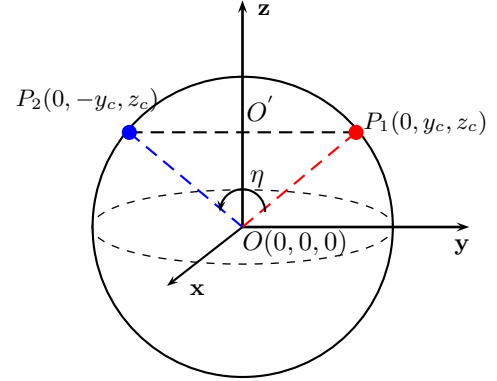


FIG. 2. Majorana representation of canonical state,  $|\psi_c\rangle$  shown as two points  $P_1$  and  $P_2$  in red and blue colors respectively. Dotted lines joining  $P_1$  and  $P_2$  with center  $O(0, 0, 0)$ , enclose angle  $\eta$  at the center of the sphere.

$\eta$  assumes values  $0 \leq \eta \leq 2\pi$ , thus the two points  $P_1$  and  $P_2$  can lie anywhere on the great circle in the plane  $x = 0$ .  $OO'$  is the perpendicular bisector of line joining the points  $P_1, P_2$  and divides the angle  $\eta$  into half. Under the action of  $U_i(\xi_i)$  transformation on spin-1 quantum state, corresponding  $OO'$  in the Majorana representation rotates like an ordinary vector in coordinate space. Depending upon the value of  $\alpha$  the magnitude of bisector  $OO'$  attains values ranging from +1 to -1 while this magnitude remains invariant under rotations. This opens up an interesting possibility of obtaining a family of states related to each other by  $SO(3)$  transformations for each value of the magnitude of  $OO'$ . It turns out that each and every state of a single qutrit can be obtained from this canonical state using  $SO(3)$  transformations.

To see this explicitly, we give a set of three  $SO(3)$  operators with specific angles and rotation axes, under whose action the spin-1 general state can be taken to the spin-1 canonical state and vice versa. Since we know that there exists a one-to-one correspondence between the operators  $U_i(\xi_i)$  in Hilbert space and  $R_i(\xi_i)$  in the coordinate space, we make use of the Majorana representation of the states  $|\psi_g\rangle, |\psi_c\rangle$  (defined in Eqn. (5) and (14) to find the set of rotation matrices  $R_i(\xi_i)$ s and then the corresponding unitary matrices.

Starting with the Majorana representation of a general state  $|\psi_g\rangle$  consisting of points  $P_1$  and  $P_2$  as depicted in Fig. 1(a) with their polar coordinate on the sphere given via Eqn.(4), we aim to rotate and go to points representing the canonical state  $|\psi_c\rangle$  which consists of a pair of points on the great circle in the plane  $x = 0$ . This is achieved by rotating the points  $P_1$  and  $P_2$  about  $y$ -axis by angle  $\gamma$  followed by a rotation  $z$ -axis by angle  $\beta$  such that both the points can be brought to the plane  $x = 0$ . Further a rotation about  $x$ -axis ( $R_x(\delta)$ ), is performed to bring the points symmetrically about the

$z$  axis to finally arrive at the configuration of points for the canonical state  $|\psi_c\rangle$ . The angles of rotations are given by:

$$\begin{aligned}\beta &= \tan^{-1} \frac{\cos \phi_1 \tan \theta_1 - \cos \phi_2 \tan \theta_2}{\sin \phi_1 \tan \theta_1 - \sin \phi_2 \tan \theta_2} \\ \gamma &= \cos^{-1} \pm \sqrt{\frac{\cos^2 \theta_1 - \cos^2 \theta_2}{\sin^2 \theta_2 \sin^2(\beta + \phi_2) - \sin^2 \theta_1 \sin^2(\beta + \phi_1)}} \\ \delta &= \tan^{-1} \frac{\cos \gamma (\sin \theta_1 \sin(\beta + \phi_1) + \sin \theta_2 \sin(\beta + \phi_2))}{\cos \theta_1 + \cos \theta_2}\end{aligned}\quad (15)$$

Corresponding operations in the Hilbert space leads us to the canonical state, starting from the general spin-1 state (or vice versa)

$$|\psi_c\rangle = U_x(\delta)U_z(\gamma)U_y(\beta)|\psi_g\rangle. \quad (16)$$

Thus, the single parameter canonical state ( $|\psi_c\rangle_\alpha$ ) along with the rotations by angles  $\beta$ ,  $\gamma$ , and  $\delta$  can be used to reach any state in the three-dimensional Hilbert space.

## B. Invariant Magnetization

When a magnetic moment is associated with a qutrit, we can associate magnetization with the corresponding angular momentum operators. For a general pure state of the qutrit  $\rho = |\psi\rangle\langle\psi|$  the magnetization vector in terms of the expectation values of  $\Sigma_i$  can be written as:

$$\vec{M} = \langle\Sigma_1\rangle\hat{x} + \langle\Sigma_2\rangle\hat{y} + \langle\Sigma_3\rangle\hat{z}. \quad (17)$$

For the canonical state  $|\psi_c\rangle$  the expectation values are

$$\langle\Sigma_1\rangle = 0, \quad \langle\Sigma_2\rangle = 0, \quad \langle\Sigma_3\rangle = -\cos(2\alpha). \quad (18)$$

and the magnitude of the magnetization vector is:

$$|\vec{M}| = |\cos(2\alpha)|. \quad (19)$$

For the eigen states of  $\Sigma_3$  the values are

$$\text{For } \alpha = 0, \quad \frac{\pi}{2} |\vec{M}| = 1, \quad \text{For } \alpha = \frac{\pi}{4}, \quad |\vec{M}| = 0. \quad (20)$$

The action of  $SO(3)$  causes rotation of spin as a whole without affecting the magnitude of the magnetization vector. Thus the amount of magnetization of a qutrit in an arbitrary state  $|\psi\rangle$  remains unaltered under  $SO(3)$ .

The magnetization finds a natural representation on the Majorana sphere where the magnetization vector or a single qutrit can be related to the bisector of the angle enclosed between the pair of points representing the state on the Majorana sphere. As per Fig. 2, the length  $l_b$  of the perpendicular bisector  $OO'$  is

$$l_b = z_c = \cos \frac{\eta}{2} = \frac{\sin \alpha - \cos \alpha}{\sin \alpha + \cos \alpha}. \quad (21)$$

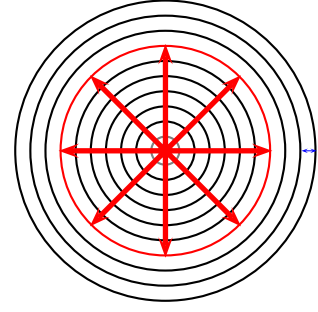


FIG. 3. Cross-sectional representation of the Majorana sphere. Circles of different radii correspond to surfaces of constant magnetization of a single qutrit. Red arrows pointing towards different directions are a few of the infinitely many magnetization vectors for a given value of the magnitude of magnetization (shown in red).

The magnetization  $\vec{M}$ , the canonical state parameter  $\alpha$  and the length of the bisector  $OO'$  are related to each other as

$$|\vec{M}| = |\langle\psi_c|\Sigma_3|\psi_c\rangle| = |-\cos(2\alpha)| = \frac{2|l_b|}{(l_b^2 + 1)} \quad (22)$$

Thus, in the context of Majorana representation,  $|\vec{M}|$  can be obtained from length  $l_b$  of the bisector  $OO'$  (Fig. 2). Under the action of  $SO(3)$  the quantities  $l_b$  and  $\frac{2|l_b|}{(l_b^2 + 1)}$  are invariant.

The magnitude of the magnetization vector  $|\vec{M}|$  in a pure ensemble of a single qutrit can assume values in the range  $[0, 1]$ . On the contrary, the pure ensemble of a qubit always possesses unit magnitude of the magnetization vector associated with it. The geometrical picture of the single qutrit magnetization vector is provided by the Majorana representation. The value  $|\vec{M}|$  depends upon the length of the bisector  $OO'$  and lies along the  $z$ -axis and is rotationally invariant. Thus corresponding to a given value of the length of the bisector, one can assume concentric spheres with continuously varying radii, whose surfaces are the surfaces of constant magnetization. The radii of these spheres are equal to  $|\vec{M}|$ , that vary in the range  $[0, 1]$ . Circular cross-section of the Majorana sphere depicting the magnetization vector is shown in Fig. 3 where an example with  $|\vec{M}| = \frac{1}{\sqrt{2}}$  is shown as a red circle inside the cross-section of a unit sphere. Depending on whether a specific direction can be assigned to the qutrit state or not, these states can be classified as ‘pointing’ or ‘non-pointing’. A single qutrit state that has a direction of orientation and also possesses a non-zero magnetization is termed a pointing state, while the states with zero magnetization content and without any directional orientation are termed non-pointing states. In the Majorana representation, non-pointing states consist of diametrically opposite points on the unit sphere, such that the bisector of the angle enclosed at the center of the sphere vanishes. On the other hand, pointing states have non-zero magnetization. Under  $SO(3)$  trans-

formations, pointing states remain always pointing while the non-pointing states remain non-pointing. For example the states  $|+1\rangle(|-1\rangle)$ , state points along  $+z(-z)$  direction. On the other hand  $|0\rangle$  has diametrically opposite points in the Majorana representation and is a non-pointing state.

In general, an eigenstate of  $\Sigma_i$  with eigenvalue  $+1$  points along the  $+i$  direction and an eigenstate of  $\Sigma_i$  with eigenvalue  $-1$  points in the  $-i$  direction. States with zero eigenvalue can be supposed to have a zero magnetization and thus do not have any preferred direction of orientation.

The canonical state of a single-qutrit undergoes a rotation under the effect of  $SO(3)$  transformations, in such a way that the magnitude of the magnetization vector remains unchanged. However  $SU(3)$  transformations change both the magnitude as well as direction of the single-qutrit magnetization vector. For instance, a unitary transformation,  $e^{-i\theta\Lambda_5}$ , transforms the coefficients of  $|+1\rangle$  and  $|-1\rangle$  of the one-parameter family of states  $|\psi_c\rangle$  in such a way that the angle  $\alpha$ . Therefore, this type of operation can be used to alter the magnetization magnitude. On the Majorana sphere, this operation corresponds to opening or closing of angle  $\alpha$  between the two points representing the canonical state of the qutrit as depicted in Fig. 2.

The magnetization for the general state  $|\psi_g\rangle$  defined in Eqn. (5) can be easily computed and turns out to be:

$$\begin{aligned}\langle\Sigma_1\rangle &= \Gamma(\sin\theta_1\cos\phi_1 + \sin\theta_2\cos\phi_2) \\ \langle\Sigma_2\rangle &= \Gamma(\sin\theta_1\sin\phi_1 + \sin\theta_2\sin\phi_2) \\ \langle\Sigma_3\rangle &= \Gamma(\cos\theta_1 + \cos\theta_2)\end{aligned}\quad (23)$$

The Majorana representation of the general single-qutrit state is given by two points:  $P_1(\sin\theta_1\cos\phi_1, \sin\theta_1\sin\phi_1, \cos\theta_1)$  and  $P_2(\sin\theta_2\cos\phi_2, \sin\theta_2\sin\phi_2, \cos\theta_2)$ . Point  $O'(x', y', z')$  bisects the chord  $P_1P_2$ , which when connected to the center of the sphere  $O$ , provides the direction of the single-qutrit magnetization vector:

$$\vec{M} = \langle\Sigma_1\rangle\hat{x} + \langle\Sigma_2\rangle\hat{y} + \langle\Sigma_3\rangle\hat{z} = \frac{2}{l_b^2 + 1}\vec{OO'}.\quad (24)$$

Thus a physical picture of the single-qutrit magnetization vector is realized with the help of Majorana representation of a qutrit. Further, one can observe the evolution of single-qutrit magnetization vector under various quantum operations.

## IV. QUANTUM COMPUTING WITH A SINGLE-QUTRIT

### A. NMR qutrit

A natural realization of a qutrit in NMR is a spin-1 nucleus, wherein the three eigenstates of the operator  $\Sigma_3$  namely  $|+1\rangle$ ,  $|0\rangle$  and  $|-1\rangle$ , split in energy in the

presence of a magnetic field as shown in Fig. 4(a) (the states are labeled as  $\{1, 2, 3\}$  for convenience). The NMR Hamiltonian of a spin-1 nucleus in the presence of a static magnetic field,  $B_0 = -\omega_0/\gamma$ , is given by [3, 37] (we have used the standard NMR notation in this section and the  $I$  operators in this section are the same as the  $\Sigma$  operators of the previous section):

$$H = -\omega_0 I_z + \frac{eQV_{zz}}{4I(2I-1)}(3I_z^2 - I^2)\quad (25)$$

where  $\omega_0$  is the Larmor precession frequency,  $\gamma$  is the gyromagnetic ratio,  $Q$  is the quadrupolar moment and  $V_{zz}$  is the average value of the uniaxial electric field gradient component over the molecular motion. The second term in the R.H.S. of Eqn. (25) is the quadrupolar coupling term, whose average vanishes in an isotropic medium as provided by liquid state NMR. Only the Zeeman interaction term survives, leading to three equally separated energy levels and an overlapped pair of spectral lines which cannot be addressed separately in frequency space. The quadrupolar coupling is retained in an anisotropic environment such as that provided by a liquid crystalline medium. The anisotropic molecular orientation with respect to the magnetic field gives rise to a quadrupolar coupling term in the Hamiltonian which is now given by

$$H = -\omega_0 I_z + \Lambda(3I_z^2 - I^2)\quad (26)$$

where  $\Lambda = e^2qQS/4$  is the effective value of the quadrupolar coupling,  $eq = V_{zz}$  denotes the field gradient parameter, and  $S$  is the order parameter of the liquid crystal. The effective quadrupolar coupling value depends upon the order parameter of the liquid crystal, and is responsible for the splitting between the previously degenerate energy levels which now gives rise to two non-degenerate spectral lines.

The spin-1 system used in this study is the deuterium spin in a deuterated chloroform molecule oriented in a lyotropic liquid crystal [32]. The lyotropic liquid crystal is composed of 25.6% of Potassium Laurate, 68.16% of  $H_2O$  and 6.24% of Decanol [38], and 50  $\mu l$  of Chloroform-D was added to 500  $\mu l$  of the liquid crystal during sample preparation. A temperature of 277 K was found to be optimal for performing the experiments (at which  $T_1$  and  $T_2$  relaxation times are approximately 170 ms and 50 ms respectively). The relative separation of the single quantum transitions is 936 Hz on a 600 MHz NMR spectrometer (as shown in Fig. 4(b)). All the experiments were performed on a 600 MHz Avance III NMR spectrometer equipped with a QXI probe, with the deuterium nucleus resonating at 91.108 MHz. All the transition-selective rf pulses used in this work are 'Gaussian' shaped pulses of 4 ms duration, while the non-selective rf pulses are 'Sinc' shaped pulses with a duration of 0.5 ms.

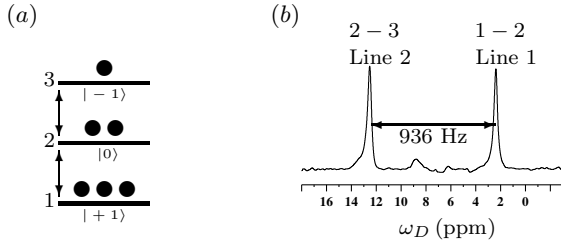


FIG. 4. (a) Single-qutrit energy level diagram depicting the thermal equilibrium population distribution of the eigen vectors labeled as  $\{|1, 2, 3\rangle$ . (b) Deuterium NMR spectrum of oriented deuterated chloroform molecule at 277 K. The spectral lines are labeled as Line 1 and Line 2. At 277 K, the anisotropic liquid crystalline environment is shown to exhibit an effective quadrupolar splitting of 936 Hz.

### B. Initialization and tomography of a single qutrit

For the purpose of NMR quantum computation, one needs to initialize the quantum system in a pseudopure state which is obtained by having a different population in one of the energy levels over a uniform background in an ensemble of  $\sim 10^{18}$  spins. A qutrit has three possible pseudopure states :  $|+1\rangle$ ,  $|0\rangle$ ,  $|-1\rangle$ , which are obtained from the thermal equilibrium state using transition-selective pulses followed by a gradient pulse that dephases the coherences [32, 35]. NMR pulse sequences for the preparation of pseudo-pure states  $|-1\rangle$ ,  $|0\rangle$ ,  $|+1\rangle$  are shown in Fig. 5(a),(b),(c) respectively.

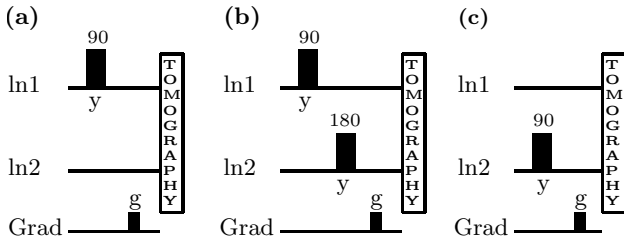


FIG. 5. Pseudopure state preparation scheme, resulting into states : (a)  $|-1\rangle$ , (b)  $|0\rangle$  and (c)  $|+1\rangle$ . Channels ln1 and ln2 correspond to transitions 1-2 and 2-3 respectively. The gradient pulse of strength  $g$  is shown in the third channel.

The final readout of the experimental state is performed by quantum state tomography. Generators of  $SU(3)$  operators ( $\Lambda$  matrices) alongwith a  $3 \times 3$  identity matrix form a complete set of orthonormal bases in the operator space of spin-1. The state of the spin-1 in general is  $\rho = \frac{1}{2} \sum_{i=1}^8 c_i \Lambda_i$  where  $c_i$ s are real numbers. State reconstruction requires all eight expectation values i.e.  $c_i$ s to be determined, which requires a minimum of four operations which are given below alongwith their corresponding NMR pulse sequences [32]:

- Identity : No operation
- $U_{\Lambda_1}(\frac{3\pi}{2}) : I_x^{1-2}(-\pi)$

- kill coherences,  $U_{\Lambda_1}(\frac{\pi}{4}) : Grad_z, I_y^{1-2}(\frac{\pi}{2})$
- kill coherences,  $U_{\Lambda_7}(\frac{\pi}{4}) : Grad_z, I_y^{2-3}(\frac{\pi}{2})$

The NMR spectrum of a qutrit contains of two lines corresponding to the single quantum coherences  $\rho_{12}$  and  $\rho_{23}$ . The first experiment in the tomography protocol outlined above gives the values of  $(c_1, c_2, c_6, c_7)$ , the second experiment interchanges the intensities of single- and double-quantum terms providing the values of  $(c_4, c_5)$  and the last two experiments give the diagonal elements and hence the values of  $(c_3, c_8)$ . Calculating all these values from the intensities of spectral lines, the experimental density matrix ( $\rho_e$ ) can be constructed. The measure of overlap used between the theoretically expected and experimentally constructed density matrices is termed the fidelity  $F$ :

$$F = \frac{Tr(\rho \dagger \rho_e)}{\sqrt{Tr(\rho \dagger \rho)} \sqrt{Tr(\rho_e \dagger \rho_e)}}. \quad (27)$$

The experimentally tomographed single-qutrit states are shown in Fig. 6. Pseudopure states  $|+1\rangle$ ,  $|0\rangle$  and  $|-1\rangle$  are obtained with the fidelities 0.99, 0.97 and 0.99 respectively.

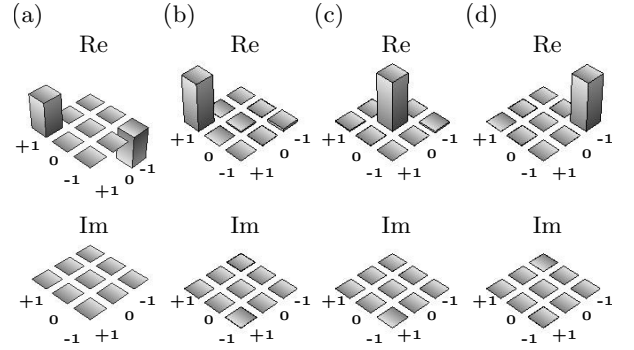


FIG. 6. Real (Re) and imaginary (Im) parts of the experimentally constructed single-qutrit density matrices are shown for (1) thermal equilibrium state, and the pseudo-pure states: (b)  $|+1\rangle$ , (c)  $|0\rangle$ , and (d)  $|-1\rangle$ . These pseudo-pure states are created using pulse sequences given in Fig. 5. The pseudo-pure states  $|+1\rangle$ ,  $|0\rangle$ , and  $|-1\rangle$  are found to have fidelities of 0.99, 0.97 and 0.99 respectively.

### C. Experimental implementation of $\Lambda$ matrices

Each of the two single-quantum transitions of an NMR qutrit belong to a two-level subspace. The transition-selective pulses in NMR are governed by transition-selective operators as described earlier (Eqn. (9)). The experimental implementations of the  $\Lambda$  matrices  $U_{\Lambda_1}$  and  $U_{\Lambda_2}$  require a selective excitation of the transition between energy levels 1, 2, while the implementations for  $U_{\Lambda_6}$  and  $U_{\Lambda_7}$  are achieved by a transition-selective radio frequency pulse between energy levels 2, 3.



The implementations for  $U_{\Lambda_4}$  and  $U_{\Lambda_5}$  require a double-quantum excitation which is achieved using a set of three transition-selective pulses [39].  $U_{\Lambda_3}$  and  $U_{\Lambda_8}$  correspond to  $z$ -rotations and can be implemented using  $z$ -cascade pulses. The NMR pulse sequences corresponding to the  $U_{\Lambda_i}(\theta)$  implementations are shown in Fig. 7. Imple-

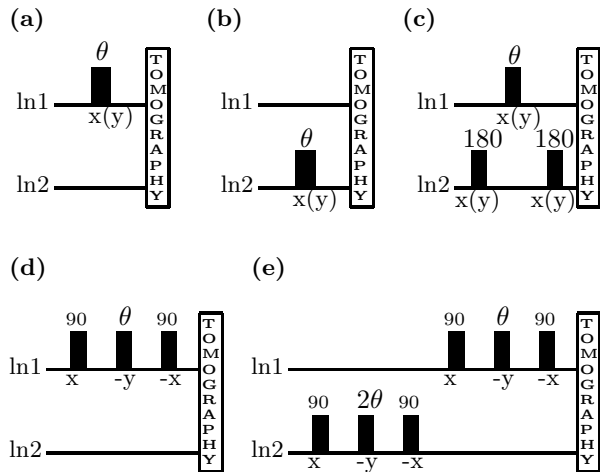


FIG. 7. NMR pulse sequence for the implementation of (a)  $U_{\Lambda_1}(U_{\Lambda_2})$  giving rotation  $\frac{\theta}{2}$ , using transition selective pulses.  $\theta = \pi$  swaps the populations between energy levels 1 and 2 of a single spin 1, (b)  $U_{\Lambda_6}(U_{\Lambda_7})$  giving rotation  $\frac{\theta}{2}$ , using transition selective pulses.  $\theta = \pi$  swaps the populations between energy levels 2 and 3, (c)  $U_{\Lambda_4}(U_{\Lambda_5})$  giving rotation  $\frac{\theta}{2}$ , using a single spin selective pulse.  $\theta = \pi$  swaps the populations between energy levels 1 and 3. Pulse sequences for the implementation of (d)  $U_{\Lambda_3}$  and (e)  $U_{\Lambda_8}$  matrices giving rise to the relative phase shifts. All the black rectangular pulses are the shaped pulses with angle of rotation mentioned at the top and the axis of rotation is mentioned at the bottom. ln1 and ln2 stand for the transitions between levels 1-2 and 2-3 respectively.

mentation of unitary transformations corresponding to  $\Lambda$  matrices on single-qutrit magnetization vector, leads to change in both its magnitude as well as direction and can be visualized on the Majorana sphere as described in the Section III B.

#### D. Quantum Gates

Similar to qubits, quantum computation with qutrits uses single-qutrit and two-qutrit operators as quantum gates. We describe below the implementation of some basic gates on an NMR qutrit.

##### 1. Chrestenson gate

The Chrestenson gate is the qutrit analog of the single-qubit Hadamard gate. It is a single-qutrit gate that creates uniform superpositions of the energy levels along with relative phases between the basis vectors. Chresten-

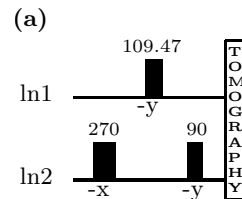


FIG. 8. Pulse sequence for Chrestenson gate implementation on qutrit pseudopure states. The two channels correspond to two transitions of a single qutrit. Pulse angles and axes are mentioned along with all the pulses.

son gate for single-qutrit is written as:

$$Ch = \frac{1}{\sqrt{3}} \begin{pmatrix} 1 & 1 & 1 \\ 1 & e^{\frac{2i\pi}{3}} & e^{\frac{4i\pi}{3}} \\ 1 & e^{\frac{4i\pi}{3}} & e^{\frac{2i\pi}{3}} \end{pmatrix} \quad (28)$$

Considering the action of Chrestenson gate on the non-pointing state  $|0\rangle$  leads to the state  $\frac{1}{\sqrt{3}} (|+1\rangle + e^{\frac{2\pi i}{3}}|0\rangle + e^{\frac{4\pi i}{3}}|-1\rangle)$ , which is a pointing state. Chrestenson gate can not be obtained solely under  $SO(3)$  transformations. Therefore, the decomposition of this gate requires a set of  $SU(3)$  operators which in turn require transition-selective pulses for NMR experimental implementation. We proposed a non-trivial sequence of rf pulses for the Chrestenson gate implementation in NMR (details given in Ref. [32]).

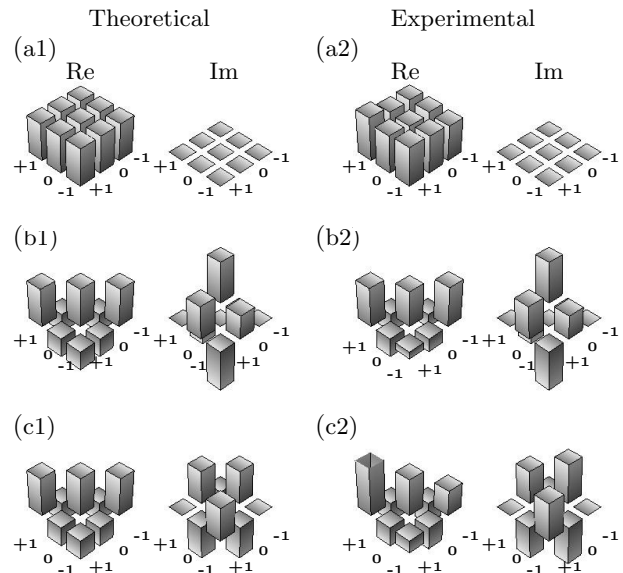


FIG. 9. Real and imaginary parts of the theoretically expected ( $a_1, b_1, c_1$ ) and experimentally obtained ( $a_2, b_2, c_2$ ) tomographs of the resultant single-qutrit state after Chrestenson gate implementation on different initial states. The initial states corresponding to different parts are: ( $a_1, a_2$ )  $|+1\rangle$ , ( $b_1, b_2$ )  $|0\rangle$ , and ( $c_1, c_2$ )  $|-1\rangle$ .

This pulse sequence is applied on all three qutrit bases states and the final state is completely tomographed.



Final state density matrices are shown in Fig. 9. As seen from the Fig. 9, theoretically expected and experimentally obtained single-qutrit states match well after the Chrestenson gate implementation. The exact overlap between the theoretically expected and experimentally obtained states (Eqn. (27)) is found out to be 0.99, 0.98, 0.98 corresponding to initial states  $|+1\rangle$ ,  $|0\rangle$ ,  $| -1\rangle$  respectively. Visualizing on the Majorana sphere, Chrestenson gate implementation on all three basis states of a single-qutrit, brings the magnetization vector to the plane  $z = 0$ . The magnetization vector of these respective final states lie symmetrically in the plane  $z = 0$  at angles of  $2\pi/3$  with respect to each other.

## 2. SWAP gates

A qutrit is a three-level system, therefore there are three possible swap operations between levels 1-2, 2-3 and 1-3. This is achieved by using transition-selective pulses. Exact pulse sequences for NMR implementation of  $\text{SWAP}_{12}$ ,  $\text{SWAP}_{23}$  and  $\text{SWAP}_{13}$  are shown in Fig 10. However for  $\theta = \pi$ , SWAP gates can effectively be implemented by the unitary operators  $U_{\Lambda_j}$ . The explicit matrices for  $\text{swap}_{12}$ ,  $\text{swap}_{23}$  and  $\text{swap}_{13}$  are written as

$$\begin{pmatrix} 0 & 1 & 0 \\ 1 & 0 & 0 \\ 0 & 0 & 1 \end{pmatrix}, \quad \begin{pmatrix} 1 & 0 & 0 \\ 0 & 0 & 1 \\ 0 & 1 & 0 \end{pmatrix}, \quad \begin{pmatrix} 0 & 0 & 1 \\ 0 & 1 & 0 \\ 1 & 0 & 0 \end{pmatrix} \quad (29)$$

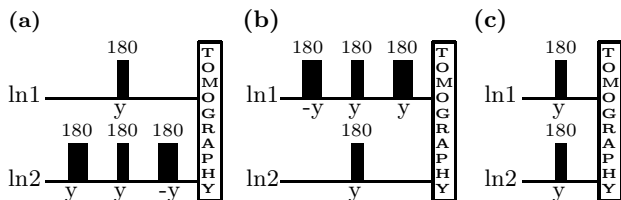


FIG. 10. Pulse sequence for implementation of swap operations. (a)  $\text{SWAP}_{12}$ , (b)  $\text{SWAP}_{23}$  and (c)  $\text{SWAP}_{13}$ . Transition selective pulses are shown by thick rectangles while thin rectangles are the non-selective pulses.

All three SWAP gates are implemented experimentally on the thermal equilibrium state. Complete quantum state tomography of all states was performed. The fidelities corresponding to  $\text{SWAP}_{12}$ ,  $\text{SWAP}_{23}$ , and  $\text{SWAP}_{13}$  implementations are 0.99, 0.99, 0.99 respectively. The tomographs of the initial and final states are shown in Fig. 11. SWAP gates are implemented on single-qutrit states, whose Majorana representation consists of two points on the unit sphere. Under  $\text{SWAP}_{12}$  gate implementation one of the points (say the first point) gets flipped and occupies the diametrically opposite position on the Majorana sphere;  $\text{SWAP}_{23}$  implementation leads to the flipping of second point in Majorana representation while under  $\text{SWAP}_{13}$  operation, both the Majorana points get flipped.

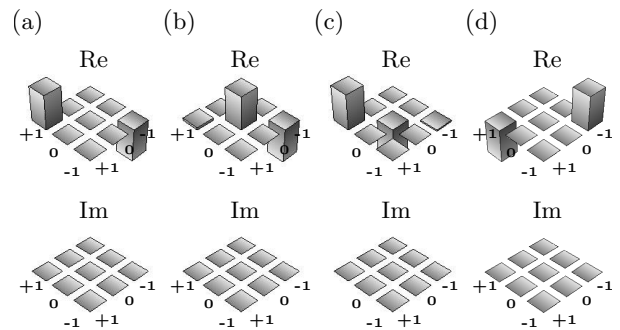


FIG. 11. Real and imaginary parts of the (a) Initial state (thermal equilibrium) and the states resulting after the implementation of (b)  $\text{SWAP}_{12}$ , (c)  $\text{SWAP}_{23}$ , and (d)  $\text{SWAP}_{13}$  operators, having state fidelities of 0.99, 0.99 and 0.98 respectively.

## 3. Phase gates

TABLE I. Phase differences between the two single quantum transitions obtained corresponding to different values of  $\theta$  under  $\Lambda_3$  and  $\Lambda_8$  implementations. Columns 3 and 4 contain the theoretically expected and experimentally obtained values of the phase difference obtained in  $\Lambda_3$  implementations, and columns 5,6 contain the theoretically expected and experimentally obtained values of the phase difference obtained as a result of  $\Lambda_8$  implementations. The angles are given in degrees.

	$\theta$	$U_{\Lambda_3}$		$U_{\Lambda_8}$	
		$\theta_{th}$	$\theta_{exp}$	$\theta_{th}$	$\theta_{exp}$
1	0	0	0	0	0
2	30	45	39.95	$30\sqrt{3}$	47
3	45	67.5	62.4	$45\sqrt{3}$	70
4	60	90	84.2	$60\sqrt{3}$	110
5	90	135	139.05	$90\sqrt{3}$	168
6	120	180	203.3	$120\sqrt{3}$	220

Phase shift gates in qutrits introduce relative phases between the base vectors of the same qutrit. These gates are primarily  $z$ -rotations and are obtained by  $U_{\Lambda_3}(\theta)$  and  $U_{\Lambda_8}(\theta)$  implementations, with their explicit matrix forms being:

$$U_{\Lambda_3} = \begin{pmatrix} e^{i\theta} & 0 & 0 \\ 0 & e^{-i\theta} & 0 \\ 0 & 0 & 1 \end{pmatrix}, \quad U_{\Lambda_8} = \begin{pmatrix} 1 & 0 & 0 \\ 0 & 1 & 0 \\ 0 & 0 & e^{i\sqrt{3}\theta} \end{pmatrix} \quad (30)$$

These gates are implemented with various values of  $\theta$ . The initial state ( $\rho_i^{exp}$ ) is created by a non-selective  $90^\circ$  pulse on thermal equilibrium state, so that one begins with in-phase values of the single quantum coherences. Action of  $U_{\Lambda_3}(\theta)$  builds a relative phase difference of  $\frac{3\theta}{2}$  between the two single quantum coherences. This

relative phase is the phase difference between the spectral lines in a single-qutrit NMR spectrum obtained by  $U_{\Lambda_3}(\theta)$  implementation on  $\rho_i^{exp}$ . The second column of the Table I shows the values of angles implemented ( $\theta$ ) as given in Fig 7(d), columns 3 and 4 contain the values of the theoretically expected ( $\theta_{th}$ ) and experimentally obtained ( $\theta_{exp}$ ) values of the phase difference respectively. A  $U_{\Lambda_8}(\theta)$  builds a relative phase difference of  $\sqrt{3}\theta$  between the two single-quantum coherences. Relative phase in the spectral lines of the first order single-qutrit spectrum under  $U_{\Lambda_8}(\theta)$  implementation ( $\theta_{exp}$ ) is shown in column 6 of the Table I, column 5 contains the theoretically expected values of phase difference ( $\theta_{th}$ ) between the two single quantum coherences.

## V. CONCLUDING REMARKS

A geometrical representation of a qutrit is described in this work, wherein qutrit states are represented by two points on a unit sphere as per the Majorana representation. A parameterization of single-qutrit states was obtained to generate arbitrary states from a one-parameter family of canonical states via the action of  $SO(3)$  transformations. The spin-1 magnetization vector was represented on the Majorana sphere and states were identified as ‘pointing’ or ‘non-pointing’ depending on the zero or non-zero value of the spin magnetization.

The transformations generated by the action of  $SU(3)$  generators were also integrated into the Majorana geometrical picture. Unlike qubits, the decomposition of single-qutrit quantum gates in terms of radio-frequency pulses is not straightforward and the Majorana sphere representation provides a way to geometrically describe these gates. Close observations of the dynamics of points representing a qutrit on the Majorana sphere under the action of various quantum gates were used to obtain the rf pulse decompositions and basic single-qutrit gates were experimentally implemented using NMR.

This work provides new insights into the intrinsic features of a qutrit with the help of Majorana representation, and introduces various NMR quantum computing protocols for a single qutrit. We think these insights will be useful to all those engaged in qutrit physics and particularly to those researchers who are exploring the use of qutrits as motifs for quantum computation.

## ACKNOWLEDGEMENTS

All experiments were performed on a 600 MHz Bruker Avance III FT-NMR spectrometer at the NMR Research Facility at IISER Mohali. Arvind acknowledges funding from DST India under Grant No. EMR/2014/000297. KD acknowledges funding from DST India under Grant No. EMR/2015/000556. SD acknowledges University Grants Commission (UGC) India for financial support.

- 
- [1] M. A. Nielsen and I. L. Chuang, *Quantum Computation and Quantum Information* (Cambridge University Press, Cambridge UK, 2002).
- [2] I. Bengtsson and K. Życzkowski, *Geometry of quantum states, majorana, geometry* (Cambridge University Press, New York, USA, 2006).
- [3] M. H. Levitt, *Spin dynamics : Basics of nuclear magnetic resonance, parity, majorana* (John Wiley and Sons, Chichester England, 2008).
- [4] Arvind, K. S. Mallesh, and N. Mukunda, *J. Phys. A* **30**, 2417 (1997).
- [5] S. K. Goyal, B. N. Simon, R. Singh, and S. Simon, *J. Phys. A* **49**, 165203 (2016), quant-ph/1111.4427v1.
- [6] S. Ashourisheikhi and S. Sirsi, *Int. J. Quant. Inf.* **11**, 1350072 (2013).
- [7] H. Mäkelä and A. Messina, *Phys. Rev. A* **81**, 012326 (2010).
- [8] H. Mäkelä and A. Messina, *Physica Scripta* **2010**, 014054 (2010).
- [9] S. Sen, M. R. Nath, T. K. Dey, and G. Gangopadhyay, *Annals of Physics* **327**, 224 (2012).
- [10] M. Planat, *Int. J. Geom. Methods Mod. Phys.* **8**, 303 (2011).
- [11] F. Yan, M. Yang, and Z. L. Cao, *Phys. Rev. A* **82** (2010).
- [12] E. Majorana, *Nuovo Cimento* **9**, 43 (1932).
- [13] J. H. Hannay, *J. Phys. A* **31**, L53 (1998).
- [14] H. D. Liu and L. B. Fu, *Phys. Rev. Lett.* **113**, 240403 (2014), quant-ph/1406.6821v2.
- [15] A. R. U. Devi, Sudha, and A. K. Rajagopal, *Quantum Information Processing* **11**, 685 (2012).
- [16] W. Ganczarek, M. Kuses, and K. Z. Życzkowski, *Phys. Rev. A* **85**, 032314 (2012).
- [17] A. R. U. Devi, Sudha, and A. K. Rajagopal, *ArXiv e-prints*, (2010), quant-ph/1002.2820v1.
- [18] A. R. U. Devi, Sudha, and A. K. Rajagopal, *ArXiv e-prints*, (2010), quant-ph/1003.2450v1.
- [19] J. H. Hannay, *J. Phys. A* **29**, L101 (1996).
- [20] J. H. Hannay, *J. Mod. Opt.* **45**, 1001 (1998).
- [21] B. Li, Z.-H. Yu, and S.-M. Fei, *Scientific Reports* **3**, 2594 (2013).
- [22] V. E. Zobov and V. P. Shauro, *J. Exp. Theo. Phys.* **113**, 181 (2011).
- [23] C. Akyz, E. Aydner, and . Mstecaploglu, *Optics Communications* **281**, 52715277 (2008).
- [24] G. Molina-Terriza, A. Vaziri, J. Rehacek, Z. Hradil, and A. Zeilinger, *Phys. Rev. Lett.* **92**, 167903 (2004).
- [25] D. Bruß and C. Macchiavello, *Phys. Rev. Lett.* **88**, 127901 (2002).
- [26] N. K. Langford, R. B. Dalton, M. D. Harvey, J. L. O’Brien, G. J. Pryde, A. Gilchrist, S. D. Bartlett, and A. G. White, *Phys. Rev. Lett.* **93**, 053601 (2004).
- [27] B. P. Lanyon, T. J. Weinhold, N. K. Langford, J. L. O’Brien, K. J. Resch, A. Gilchrist, and A. G. White, *Phys. Rev. Lett.* **100**, 060504 (2008).
- [28] A. Peres, *J. Phys. A* **24**, L175 (1991).
- [29] S. Yu and C. H. Oh, *Phys. Rev. Lett.* **108**, 030402 (2012).

- [30] P. Kurzynski and D. Kaszlikowski, Phys. Rev. A **86**, 042125 (2012).
- [31] T. D. Ladd, F. Jelezko, R. Laflamme, Y. Nakamura, C. Monroe, and J. L. O'Brien, Nature **464**, 45 (2010).
- [32] S. Dogra, Arvind, and K. Dorai, Phys. Lett. A **378**, 3452 (2014).
- [33] Z. Gedik, I. A. Silva, B. Cakmak, G. Karpat, E. L. G. Vidoto, D. O. Soares-Pinto, E. R. deAzevedo, and F. F. Fanchini, Scientific Reports **5**, 14671 (2015).
- [34] T. Gopinath and A. Kumar, Phys. Rev. A **73**, 022326 (2006).
- [35] R. Das, A. Mitra, V. S. Kumar, and A. Kumar, Int. J. Quant. Inf. **1**, 387 (2003).
- [36] A. Wokaun and R. R. Ernst, J. Chem. Phys. **67**, 1752 (1977).
- [37] C. P. Slichter, *Principles of Magnetic resonance*, parity, majorana (Springer, Newyork, 1996).
- [38] L. J. Yu and A. Saupe, Phys. Rev. Lett. **45**, 1000 (1980).
- [39] K. Dorai and A. Kumar, J. Magn. Reson. **114 A**, 155 (1995).